

# Nonlinear power law modeling for test vehicle structural response

Jai Singh<sup>1</sup>

<sup>1</sup>Biomechanical Engineering Analysis & Research, Inc.  
2060-D Avenida de los Arboles, No. 487, Thousand Oaks, California 91362, USA

\*\*\*

**Abstract** - *The full width engagement impact between the front of a test vehicle and a fixed, rigid, massive barrier represents a common, if not the most common, collision configuration within the context of controlled testing conducted for safety standard compliance or assessment purposes. In cases in which the barrier is instrumented and with the instrumentation specifically including a load cell array comprised of a sufficient number of individual load cells aligned along the principle test direction, the structural response of the test vehicle during the impact can be characterized within the context of a single degree of freedom, ubiquitously collinear modeling approach without reliance upon any test vehicle affixed instrumentation. This characterization, based upon the time-parametric force deflection response, is generally nonlinear for both the closure and separation phases of the collision. Investigated in the subject work, for the totality of each phase, is the use of nonlinear power law formulations for modeling the force-deflection response. A criterion is developed, based upon the peak deflection, peak collision force and internal work absorbed in regards to a set of closure phase responses for which such a modeling approach is appropriate. Three distinct power law models are developed and presented in regards to the modeling of separation phase responses. These models are compared to extant, linear, phasic response models.*

**Key Words:** Collision testing, nonlinear modeling, power law models

## 1. INTRODUCTION

One may define a collision as the physical phenomenon that occurs when two or more distinct objects (or two or more distinct aspects of the same object) attempt to simultaneously occupy the same region of physical space. The kinematic and kinetic responses that arise from the physical phenomenon in question define a set of metrics that are the most objective when it comes to representing the severity of the event. The accurate quantification of these metrics is a typical and common component of the engineering endeavor of vehicular collision reconstruction. The phrase vehicular collision reconstruction, rather than accident reconstruction, is used herein due to the basic fact that the physical phenomenon in question and the framework utilized for understanding and modeling the physical phenomenon in question (i.e. the episteme) is entirely intransient to legal precepts of human intention.

Within the context of vehicular collision reconstruction, advances in the composite field of vehicle electronics coupled with their broad adaptation has resulted in the establishment of a new paradigm. This paradigm is one of quantifying certain collision severity metrics based upon retrieval of data, from the vehicular collision partner itself, which in turn was generated during the collision and subsequently stored. Certain situations, including but not limited to, cases involving collision partners for which such system(s) were not included at the time of manufacture, the lack of coverage for data extraction using aftermarket, commercially available hardware and software systems, data loss, lack of vehicle availability or any combination of the aforementioned results in the necessity for relying upon other methods for estimating the salient quantifiable collision severity metrics. One class of such methods involves the analysis of evidence generated during a collision event, the relatively immediate temporal period surrounding a collision event or both. An example is the deposition of tire mark evidence, on a roadway, secondary to vehicle operator mediated braking, steering or both. Cases in which such evidence is present, antecedent to a collision event, specifically due to operator mediated brake application, however, has become an increasing rarity secondary to the near ubiquitous inclusion of anti-lock brakes as a standard vehicle feature. In most cases, the salient evidence generated is that which occurred during a collision and consists of the residual damage present to the vehicular collision partners.

The importance of residual damage analysis based methods for quantifying collision severity metrics cannot be understated. In the United States, the National Center for Statistics and Analysis (NCSA), of the National Highway Traffic Safety Administration (NHTSA), has been involved in the collection of motor vehicle traffic collision data through the National Automotive Sampling System/Crashworthiness Data System (NASS/CDS) for over forty years. For any given traffic collision subject to such an investigation, inclusion within the NASS/CDS requires the determination and coding of the collision phase velocity change for the salient vehicular collision partners. In this regard, the collision phase velocity change ( $\Delta v$ ) is the metric by which collision severity is quantified and with such determinations predicated upon reconstruction of the collision event. As of 2007, the vast majority of coded velocity changes within the NASS/CDS were based upon residual damage analysis [1].

The phrase, residual damage, which was used in the two preceding paragraphs, requires a working definition. As used in this work, the phrase refers to the quantifiable dimensions of the permanent deformation present to a vehicular collision partner and with such deformation arising from a collision event. The reasoning behind using residual damage as the starting point in quantifying collision severity, is elementary. As the collective independent variable, in a reconstructive analysis, residual damage does not require any measurements during the collision itself. Furthermore, the dimensions of a vehicular collision partner, in the post-collision configuration, can readily be ascertained, even well after the incipient collision event, and through a number of different means. Dimensional data regarding an undeformed reference configuration is readily available for virtually every single production vehicle. The dimensional differences between the reference and post-collision configurations define the residual damage profile.

The process of using a given residual damage profile, for a given vehicular collision partner, to quantify the severity of the collision that produced the residual damage profile, clearly requires mathematical modeling. In a general sense, a mathematical model converts a set of inputs (the independent variables) into a set of desired outputs (the dependent variables) by means of its form and generally with the use of model specific parameters. These parameters, furthermore, generally require *a priori* quantification prior to model utilization for a given case of interest. Advancing from this general statement to one of specificity in regards to the residual damage analysis for vehicular collision reconstruction, there are two empirically-based and interrelated mathematical models that have enjoyed long-standing utilization. Both models are intrinsically uniaxial and not time parametric. Based upon controlled collision testing, in a collinear configuration, in which a fixed, rigid, massive barrier (FRMB) was impacted, in each test, by the front of a test vehicle, in a full frontal width engagement impact, Campbell [2-3] postulated a linear relationship between the speed of impact and the uniaxial depth of residual deformation (i.e. crush) present to the test vehicle. Campbell generalized this finding by defining the equivalent barrier speed (EBS) as 'a vehicle velocity at which the kinetic energy of the vehicle would equal the energy absorbed in plastic deformation' and by indicating that the EBS was a linear function of the uniaxial residual damage depth.

$$\text{EBS} = b_0 + b_1 c \quad (1)$$

In equation (1), the model parameters  $b_0$  and  $b_1$  are typically referred to as the Campbell model coefficients. The term  $b_0$  represents the maximum EBS that results in a zero valued residual damage depth ( $c$ ) and the term  $b_1$  is the slope of the linear relationship. The second empirical relationship, postulated by Campbell [3] but most commonly associated with McHenry [4] was of a linear response in the collision

force magnitude, normalized per unit length of direct contact damage, and the uniaxial depth of residual damage.

$$\frac{|F|}{L} = A + Bc \quad (2)$$

In equation (2),  $|F|$  is the magnitude of the collision force,  $L$  is the length of direct contact damage,  $A$  is the maximum normalized collision force that results in a zero valued residual damage depth and  $B$  is the slope of the linear relationship. The length of direct contact damage is taken as being time invariant with respect to the collision (i.e., the value for  $L$  is taken as being the same in the reference and residual damage configurations). The model parameters  $A$  and  $B$  are commonly referred to as the CRASH3 (the acronym deriving from the third iteration of the Calspan Reconstruction of Accident Speeds on the Highway model) coefficients. The parameters from both models are collectively referred to as stiffness coefficients.

It is relevant, at this point in the presentation, to note the fact that collisions are not instantaneous events (this does not preclude the ability to accurately model collisions as such). For the vast majority of collisions of the type of interest, excluding certain sideswipe type collisions, the finite collision duration can be divided into two phases. The closure phase initiates at the first point in time that the collision partners seek to occupy the same region of physical space and terminates at the point in time in which the collision partners achieve a common velocity. The second phase, the separation phase, initiates contemporaneously with the terminus of the closure phase and terminates at the first point in time at which the collision force magnitude reaches zero. The collision force is internal to the collision partner system. During closure, the work done by the collision force is absorbed (IWA) and during separation, the work done by the collision force is recovered (IWR). The difference between the IWA and the IWR is the internal work dissipated (IWD).

These definitions are of import to the subject work. Equations (1) and (2) both relate an independent variable that is a terminus of separation variable to a dependent variable that is a terminus of closure variable (one may write the second relationship on an average basis, however, such would not be correct in regards to the work-energy relationship discussed subsequently). The CRASH3 model was explicitly developed for the closure phase. The lack of inclusion of a separation phase is functionally equivalent to treating the IWR, the coefficient of restitution (the ratio of the separation velocity to the closing velocity) and the separation velocity as being zero valued. The kinetic energy associated with the EBS from equation (1) can be obtained simply as:

$$\frac{1}{2} m \text{EBS}^2 = (b_0 + b_1 c)^2 \quad (3)$$

Equation (2) has been traditionally treated as if it were a time parametric force-deflection response. Double integration of this equation over  $L$  and  $c$  has been taken as producing an energy that is equal to that of equation (3). The integrated result is a quadratic in  $c$ , which means that the equality holds when the polynomial coefficients for each order of  $c$  (i.e.,  $c^0$ ,  $c^1$  and  $c^2$ ) are equal. This approach allows for a set of equations that relate the parameters of the two models and for which one need only estimate a value for  $b_0$ , for a given value of  $c$ ,  $L$  and EBS, in order to quantify the remaining three parameters.

The modeling of collisions in which the collision partners 'stick together' with no recovery of IWA may be appropriate for certain impact situations. However, even for the FRMB impact case described previously, the case of a test vehicle coming to rest against the barrier face is not one that is seen empirically. From the mathematical modeling perspective, for the closure phase of a collinear impact, the modeling of each deformable collision partner as a single degree of freedom (SDOF) model comprised of a single lumped mass coupled to a single, linear, relative displacement element (i.e. linear spring) can readily be found in the early literature [5] and as part of the formative basis of the CRASH3 damage analysis algorithm [4].

The question of whether or not a dynamic model containing both the closure and separation phases could be developed that (a) could account for the ordinate offsets of the empirical models and (b) maintain the linearity of the empirical models for collisions resulting in non-zero valued residual damage depths was previously addressed by the subject author [6]. Three findings from the cited work, for an affirmative response, are salient. The first finding was that the closure phase force-deflection response had to be uniformly and ubiquitously linear. The second finding was that an elastic limit, defined as a specific value of  $|F|$ , EBS or IWA was needed. Collisions at a severity up to and including the elastic limit values resulted in a non-linear separation phase response that terminated at the origin of the force-deflection curve. For such collisions, the separation phase response could not be linear as the only linear path was a reverse traversal of the linear closure phase response, thereby producing full recovery of the IWA (equivalently, a separation velocity magnitude being equal to the closing velocity magnitude and a unity valued coefficient of restitution). The non-linear response allowed for both a zero valued residual damage depth and a coefficient of restitution with less than unity valuation. The third finding was that for collisions exceeding the elastic limit, the separation phase had to be uniformly and ubiquitously linear with a force-deflection response slope of greater magnitude than the closure phase response. Any nonlinearity or multilinearity in the response for collisions exceeding the elastic limit were patently manifest in the relationship between any terminus of closure phase parameters and the depth of residual damage.

The linear model for the separation phase, as described above, however, tends to be problematic when it comes to the FRMB impact case under consideration due to the fact that it results in an overestimation of the IWR. One approach to deal with this issue, as found in the literature, has been to interpose a modeled path, for the force-deflection response, from the start of the separation phase, having infinite slope, and terminating at a normalized force value such that the subsequent finite slope response produces an IWR that matches the value determined from testing [7-10]. In the view of the subject author, this approach is unjustified, even as a modeled response. While it produces linearity in regards to the residual damage relationships and matches the IWR, the modeling approach requires a time parametric drop in force magnitude, from peak value, while the time parametric deflection remains at peak value. There is no physical phenomenon that would serve as basis for this requirement.

Returning to the scope of residual damage based models, it should be noted that other models have been proposed. Other, linear, models include a constant force model [7], a saturation force model (finite linear slope followed by zero slope region) [7] and a bilinear model [7, 11]. A non-linear power law model has also been proposed [12]. It is important to note that these models retain the non-time parametric nature of the original residual damage based models.

The non-linear power law model, as a dynamic model, has been explored previously, by the author, for modeling the closure phase [13] as well as the separation phase [14], for the FRMB impacts of interest. The objective of the subject work is the further exploration of this modeling approach within the FRMB impact context. Two points regarding the choice of this context are worthy of note. The first, being rather obvious, is that controlled collision testing provides one of the most comprehensive sources of data when it comes to quantifying model parameters. Secondly, the subject FRMB impact context is one that is incumbent in testing conducted for United States (US) Federal Motor Vehicle Safety Standard (FMVSS) 208D frontal impact compliance requirements, US high-speed frontal impact New Car Assessment Program (NCAP) testing and for testing conducted for research purposes. Collectively, testing of this type represents a significant component of all testing conducted by various contracted groups, on behalf of NHTSA.

## 2.THEORY

Within the context of understanding a given physical phenomenon of interest, it can readily be stated that a purpose of employing mathematical modeling is to engender tractability. This, in turn, consists of (a) defining a set of variables that serve as inputs, (b) defining a set of variables that serve as outputs and (c) defining the operative

relationships between these variables. There is generally a correlation between increasing levels of model complexity and the ability for modeling more aspects of the phenomenon, modeling a given aspect to a greater level of detail or both. The downside is that more complex models typically involve additional parameters and require additional data when compared to simpler models. Finally, it should also be noted that great care must be taken in employing models for situations that are beyond the strictures of the model.

With this caveat established, we can consider the graphical depiction of a collinear collision between two collision partners as shown in Figure 1. Because the problem is formulated as a collinear impact in  $R^1$  for the entirety of the collision event, the single axis of the inertial frame of reference,  $X$ , is aligned with the single axis,  $x_1$  and  $x_2$ , of each collision partner for all times of interest. This formulation, in and of itself, properly references vectors in each body frame to the inertial frame of reference. Equivalently, this can also be stated as the direction cosine matrix (DCM) that transforms vector components from each body frame to the inertial frame of reference is time invariant as the identity matrix (this also holds for the inverse transform).

$${}^G R_{B_1}(t) = I \quad {}^G R_{B_2}(t) = I_3 \quad \forall t \quad (4)$$

This does not hold for the case of general planar motion or general spatial motion.

Each collision partner is modeled as a single lumped mass coupled to a massless force carrying member. The latter represents the modeled structural properties, for the impacted region, for each collision partner. Because the spatial dimension of the problem is one, each collision partner has a single degree of freedom, which is translational along the  $X$ -axis. This single degree of freedom is parameterized by translational displacement and is denoted as  $\mathbf{u}_1(t)$  for the first collision partner and  $\mathbf{u}_2(t)$  for the second collision partner. We seek to define the modeled structural response characteristics of each collision partner, independently, rather than in the effective sense. This results in use of a massless node, representing the common collision interface, with displacement  $\mathbf{u}_{IV}(t)$ .

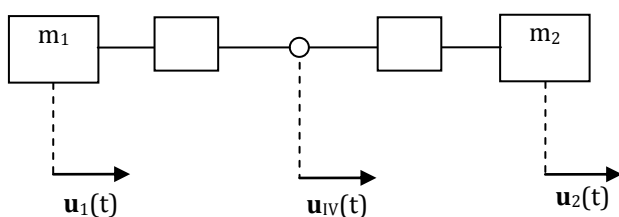


**Fig -1:** Introductory collision model

We define the deflection for each collision partner as the relative displacement between the center of mass of the same and the common collision interface. This is a direct measure of the dimensional change experienced by the massless element for each collision partner.

$$\begin{aligned} \delta_1(t) &= \mathbf{u}_1(t) - \mathbf{u}_{IV}(t) \\ \delta_2(t) &= \mathbf{u}_{IV}(t) - \mathbf{u}_2(t) \end{aligned} \quad (5)$$

This rather simple model may be reduced even further due to the modeled nature of the FRMB. Because the FRMB is fixed, it experiences no displacement during the collision event. Because the FRMB is rigid, it experiences no deflection during the collision event. Finally, because the barrier face is the common collision interface, the displacement of the same is zero. The two equations under (5) reduce to one singular operative equation for this case.

$$\delta_1(t) = \mathbf{u}_1(t) \quad (6)$$

For this case, the displacement experienced by the vehicle's center of mass, during the collision, equals the structural deflection experienced by the vehicle. This does not hold if the opposing collision partner is deformable. References in the literature and elsewhere to phrases such as 'force-displacement response,' when referencing the force-deflection response, are only correct when equation (6) holds.

There are a number of statements that can readily be made without crystallizing the form of the force-deflection model. The application of Newton's second law of motion to the vehicle yields the general form of the equation of motion for the test vehicle.

$$m_1 \ddot{\mathbf{u}}_1(t) = -\mathbf{F}(t) \quad (7)$$

Where  $m_1$  is the mass of the test vehicle,  $\mathbf{F}(t)$  is the time varying collision force (the sole force considered during the collision and internal to the two collision partner system) and the standard overdot notation is employed for representing simple time derivatives. When the FRMB is a load-cell barrier in which each load cell measures force axially, the collision force can be directly obtained by summing, at each point in time, the force measured by each load cell. This holds for the model because of the time invariant orientation noted previously and the treatment of the barrier as being rigid. The time varying force on the test vehicle is equal in magnitude but opposite in direction by Newton's third law. The second statement is that the equations for the IWA and the IWR for the two collision partner system [15] reduce by considering the mass of the FRMB in the limit.

$$IWA = \frac{1}{2} \frac{m_1 m_2}{m_1 + m_2} \mathbf{v}_c^2 \xrightarrow[m_2 \rightarrow \infty]{} IWA = \frac{1}{2} m_1 \mathbf{v}_c^2 \quad (8)$$

$$IWR = \frac{1}{2} \frac{m_1 m_2}{m_1 + m_2} v_s^2 \xrightarrow[m_2 \rightarrow \infty]{} IWR = \frac{1}{2} m_1 v_s^2 \quad (9)$$

Where  $v_c$  is the closing velocity and  $v_s$  is the separation velocity, which are defined as:

$$v_c = \dot{u}_1(t_o) - \dot{u}_2(t_o) = \dot{u}_1(t_o) - \mathbf{0} = \dot{u}_1(t_o) \quad (10)$$

$$v_s = \dot{u}_1(t_s) - \dot{u}_2(t_s) = \dot{u}_1(t_s) - \mathbf{0} = \dot{u}_1(t_s) \quad (11)$$

In equation (10), the time value  $t = t_o$  denotes the time at which the closure phase initiates. The closure phase terminates at  $t = t_c$ . For this collision configuration, a common velocity is reached, for the collision partners, at the terminus of closure. Clearly, this common velocity,  $v_{com}$ , is equal to zero due to the aforementioned modeled properties of the FRMB. In equation (11), the time value  $t = t_s$  denotes the time at which the separation phase terminates. In both equations the velocity the FRMB is zero, thereby leading to the reduction shown to the right of the last equality in each equation. The relationships shown in equations (7) - (11) are derived without any presumption regarding the nature or form of the force-deflection response of the test vehicle and hold regardless of the nature or form of the force-deflection response of the test vehicle.

We now proceed with the consideration of specific force-deflection models. The linear model, serving as comparison, for the subject nonlinear power law model, requires review.

## 2.1 Linear closure phase force-deflection model

The linear model derives its name as a result of the collision force being modelled as a linear function of the deflection.

$$F(t) = k\delta_1(t) = ku_1(t) \quad (12)$$

The form to the right of the final equality in this equation is based upon equation (6). Substitution of equation (12) into equation (7) followed by algebraic rearrangement leads to the operative second order linear differential equation of motion for the linear closure phase model.

$$m_1 \ddot{u}_1(t) + ku_1(t) = 0 \quad (13)$$

For this model, the length of the massless element, at  $t_o = 0$  is taken as being equal to the reference length of the element (i.e. the length at which the element carries zero force). This allows for an initial condition of  $u_1(0) = u_{1o} = \mathbf{0}$ . The other initial condition is of a finite, non-zero, initial velocity,  $v_1(0) = v_{1o}$ , for the test vehicle. The time domain kinematic solutions for the closure phase, for this model, are [14]:

$$u_1(t) = v_{1o}\omega^{-1} \sin(\omega t) \quad (14)$$

$$\dot{u}_1(t) = v_{1o}\cos(\omega t) \quad (15)$$

$$\ddot{u}_1(t) = -v_{1o}\omega \sin(\omega t) \quad (16)$$

Where the closure phase circular frequency,  $\omega$ , is equal to the real root of  $(k/m_1)^{0.5}$ . The time at which closure terminates is determinable from equation (15) and by knowing that the velocity of the test vehicle, at that point, is the common velocity, which is zero. Because the initial velocity is known to be non-zero valued, the equation holds when the cosine term is zero valued. Because the cosine function is periodic, it is the first solution that is used. This leads to a solution of  $t_c = \pi/(2\omega)$ . Substitution of this result into equation (14) leads to a terminus of closure displacement and deflection of  $u_1(t_c) = u_{1c} = \delta_1(t_c) = \delta_{1c} = v_{1o}\omega^{-1}$ . Similarly, the terminus of closure acceleration is determinable as  $-v_{1o}\omega$ . We may also show that the model is linear by multiplying the acceleration by the mass of the test vehicle and dividing by the deflection.

$$\frac{-F(t)}{\delta_1(t)} = \frac{m_1 v_{1o} \omega \sin(\omega t)}{v_{1o} \omega^{-1} \sin(\omega t)} = m_1 \omega^2 = m_1 \frac{k}{m_1} = k \quad (17)$$

The modeled IWA during closure can be determined by integrating the dot product of the collision force and the differential of the deflection.

$$IWA = \int_0^{t_c} F(\delta_1(t)) \cdot d\delta_1(t) = \frac{1}{2} k \delta_{1c}^2 \quad (18)$$

For any given collision test, the terms  $m_1$ ,  $v_{1o}$  and the IWA, as per equation (8) are known. The value of  $t_c$  can be determined from equation (7) by using the total barrier force to first solve for the discrete acceleration-time history, followed by numerical integration to determine the discrete velocity-time history and then determining the time at which zero velocity is reached. The discrete displacement-time history can be determined by numerical integration of the discrete velocity-time history. The terminus of closure displacement (here equal to deflection), acceleration and force values can then be determined by simply noting the value at  $t = t_c$ . Thus far, none of the values noted rely upon a model for the force deflection response. When we consider the linear closure phase model, we can readily note that the system is overdetermined once the previously listed terms are known. There are a number of solution approaches that can be employed.

1. Use the measured value of  $\delta_{1c}$  and solve for  $\omega$  using  $\omega = v_{1o}/\delta_{1c}$ . Then solve for  $k$  using  $k = m_1/\omega^2$ . Solve for the modeled value of  $F_c$  using  $F_c = k\delta_{1c}$ . Solve for the modeled value of  $t_c$  using  $t_c = \pi/(2\omega)$ .
2. Use the measured value of the force  $F_c$  to solve for the acceleration at the terminus of closure. Solve for the circular frequency by dividing the terminus of closure acceleration by  $-v_{1o}$ . Solve for  $k$  using  $k = m_1/\omega^2$ . Solve for the modeled value of  $t_c$  using  $t_c = \pi/(2\omega)$ .
3. Use the measured data point  $\{\delta_{1c}, F_c\}$  to solve for  $k$  using  $k = (F_c - F_o)/(\delta_{1c} - \delta_{1o}) = F_c/\delta_{1c}$ . Solve for  $\omega$  as above and solve for the modeled value of  $t_c$  as above.

4. Use the measured value of  $t_c$  to solve for  $\omega$  using  $\omega = \pi/(2t_c)$ . Solve for  $k$  using  $k = m_1/\omega^2$ . Solve for the modeled values of  $\delta_{1c}$  as  $v_{10}\omega^{-1}$ , the terminus of closure acceleration as  $-v_{10}\omega$  and the terminus of closure force as  $-m_1v_{10}\omega$ .

## 2.2 Power law closure phase force-deflection model

The power law models for both phases are expressed as force as a function of deflection. Both the force and the deflection are time parametric. This time parametric nature, denoted as  $(t)$ , is not shown, in certain situations, in the following derivation, simply for the purposes of clarity. It should not be forgotten that this time dependence is patent. With this noted, the closure phase power law model is:

$$F = a_0 \delta_1^{a_1} = a_0 u_1^{a_1} \quad (19)$$

The form to the right of the last equality again derives from equation (6). Equation (19) correctly produces an initial zero valued force at an initial zero deflection (at an initial zero displacement). It should also be apparent that this equation is log-linear. For two operands  $x$  and  $y$ , a power  $p$ , and a logarithm of base  $b$ , the following product, quotient, power and root identities hold.

$$\log_b(xy) = \log_b(x) + \log_b(y) \quad (20)$$

$$\log_b(xy^{-1}) = \log_b(x) - \log_b(y) \quad (21)$$

$$\log_b(x^p) = p \log_b(x) \quad (22)$$

$$\log_b \sqrt[p]{x} = p^{-1} \log_b(x) \quad (23)$$

The logarithm and exponentiation are related by the following, where  $b$  is a positive, real number:

$$\log_b(b^y) = y \quad (24)$$

For the subject work, the base,  $b$ , for all evaluations is set to Euler's number,  $e$ , and the logarithms are noted as the natural logarithm. This choice is made due to common usage and does not reduce the generality of the derivation secondary to the fact that one may readily convert a logarithm from one basis to another using the following:

$$\log_b(x) = \frac{\log_e(x)}{\log_e(b)} \quad (25)$$

With these preliminaries established, taking the natural log of equation (19) leads to the following:

$$\ln(F) = \ln(a_0 \delta_1^{a_1}) = \ln(a_0) + a_1 \ln(\delta_1) \quad (26)$$

The slope-intercept appearance of this equation is patent. A point of importance to note is the fact that  $\ln(0)$  is equal to negative infinity. Now, if equation (19) is substituted into

equation (7), it can readily be seen that the resultant equation of motion is non-linear.

$$m\ddot{u}_1(t) + a_0(u_1(t))^{a_1} = 0 \quad (27)$$

A closed form solution for equation (27) is not determinable using the methods that are appropriate for solving linear differential equations. We further note that the closure phase model has two parameters ( $a_0$  and  $a_1$ ), unlike the linear model, which has a single parameter, and thus requires two equations in order to solve for both parameters. One approach would be to write equation (19) at the terminus and at the start of the closure phase. This, however, is insufficient, due to the fact that the latter reduces to  $0 = 0$ . A second approach would be to write this equation at any two points,  $t = t_a$  and  $t = t_b$ , for which the deflection and force are not zero valued. One could then solve for the model parameters as:

$$a_1 = \ln\left(\frac{F_a}{F_b}\right)\left(\ln\left(\frac{\delta_{1a}}{\delta_{1b}}\right)\right)^{-1} \quad (28)$$

$$a_0 = F_a \delta_{1a}^{-a_1} = F_b \delta_{1b}^{-a_1}$$

Finally, and one may use the modeled IWA to determine a second equation. For this model and case, the IWA is:

$$IWA = \int_0^{\delta_{1c}} F \cdot d\delta_1 = \int_0^{\delta_{1c}} a_0 \delta_1^{a_1} \cdot d\delta_1 = \frac{a_0}{a_1 + 1} \delta_{1c}^{a_1 + 1} \quad (29)$$

We may rewrite the form on the right of the last equality by separating the exponentiated term.

$$IWA = \frac{a_0 \delta_{1c}^{a_1}}{a_1 + 1} \delta_{1c} = \frac{F_c}{a_1 + 1} \delta_{1c} \rightarrow a_1 = \frac{F_c \delta_{1c}}{IWA} - 1 \quad (30)$$

Equation (30) is the preferred initiating power law modeling equation for the closure phase. The IWA is known as per equation (8) and  $\delta_{1c}$  and  $F_{1c}$  are determinable from the data. Furthermore, the equation has only one unknown, the power,  $a_1$ . Clearly,  $a_1 \geq 0$  in order to avoid a singularity at  $\delta = 0$ . We further note that  $a_1 > 0$  is more apt secondary to the fact that the deflection raised to a zero power produces a solution of unity for all relevant deflection values. This constraint, in turn, as per equation (30), requires that  $F_c \delta_{1c}/IWA > 1$ . When this holds and when the power is known, the coefficient,  $a_0$ , can be solved for by writing equation (19) at the terminus of closure and solving directly.

Finally, if one considers two points during the closure response  $\{\delta_1, F_1\}$  and  $\{\delta_2, F_2\}$ , where neither the deflection nor the force is zero-valued, the corresponding IWA is:

$$\begin{aligned}
IWA &= \int_{\delta_1}^{\delta_2} a_0 \delta^{a_1} \\
&= \frac{a_0}{a_1 + 1} (\delta_2^{a_1+1} - \delta_1^{a_1+1}) \\
&= \frac{1}{a_1 + 1} (a_0 \delta_2^{a_1} \delta_2 - a_0 \delta_1^{a_1} \delta_1) \\
&= \frac{1}{a_1 + 1} (\mathbf{F}_2 \delta_2 - \mathbf{F}_1 \delta_1)
\end{aligned} \tag{31}$$

### 2.3 Linear separation phase force-deflection model

The separation phase terminates at the first point in time, after the terminus of the closure phase, at which the collision force returns to zero. Since the total barrier force is known, the value of  $t_s$  can be directly determined from the data. The terminus of separation acceleration, velocity and displacement can then be determined in the same manner as was discussed for the terminus of closure. With the terminus of separation velocity known, the IWR can be determined using equation (9). Again, no force-deflection model is needed to make these determinations.

For the linear model for the separation phase, a model for which closed form analytic solutions for the kinematic responses are determinable, the solution process is aided by implementing a new temporal variable,  $\tau$ , where  $\tau = t - t_c$ . As a result,  $\tau_0 = t_c - t_c = 0$  and  $\tau_s = t_s - t_c$ . One may wish to use equation (13) with a replacement of  $t$  by  $\tau$  and using the terminus of closure displacement and velocity as the initial conditions. Such an approach, however, does not result in a correct, complete set, of kinematic equations. Instead, the correct equation of motion is [14]:

$$m_1 \ddot{\mathbf{u}}_1(\tau) + \bar{k} \mathbf{u}_1(\tau) = m_1 \ddot{\mathbf{u}}_{1c} + \bar{k} \mathbf{u}_{1c} \tag{32}$$

In this equation, the terms on the right side are evaluated at  $\tau_0 = 0$  (i.e. they are the terminus of closure acceleration and displacement). Model parameters with an overbar specifically denote separation phase model parameters. The kinematic solutions are readily determinable as [14]:

$$\mathbf{u}_1(\tau) = \mathbf{u}_{1c} + \dot{\mathbf{u}}_{1c} \bar{\omega}^{-2} (1 - \cos(\bar{\omega}\tau)) \tag{33}$$

$$\dot{\mathbf{u}}_1(\tau) = \dot{\mathbf{u}}_{1c} \bar{\omega}^{-1} \sin(\bar{\omega}\tau) \tag{34}$$

$$\ddot{\mathbf{u}}_1(\tau) = \dot{\mathbf{u}}_{1c} \cos(\bar{\omega}\tau) \tag{35}$$

In these equations, the separation phase circular frequency is the positive real root of the following:

$$\bar{\omega} = (\bar{k} m)^{0.5} \tag{36}$$

The modeled value for  $\tau_s$  is based upon the acceleration response. Because the terminus of closure acceleration is not zero valued, the cosine term must be zero-valued for the

acceleration to be zero at the terminus of separation. This occurs at:

$$\tau_s = \pi (2\bar{\omega})^{-1} \tag{37}$$

The modeled terminus of separation displacement and velocity are obtained by substitution of this solution into equations (33) and (34) respectively.

$$\mathbf{u}_{1s} = \mathbf{u}_{1c} + \dot{\mathbf{u}}_{1c} \bar{\omega}^{-2} \quad \dot{\mathbf{u}}_{1s} = \dot{\mathbf{u}}_{1c} \bar{\omega}^{-1} \tag{38}$$

For the force-deflection response, we first consider a linear function  $y = f(x)$  that has a value  $y_a = f(x_a)$  and where  $x \geq x_a$ . The definition of the slope of the linear function allows the equation to be written in the following manner:

$$\text{slope} = \frac{y - y_a}{x - x_a} \rightarrow y = y_a + \text{slope}(x - x_a) \tag{39}$$

One may take a similar approach for the case where  $y_b = f(x_b)$  and where  $x_b \geq x$ .

$$\text{slope} = \frac{y_b - y}{x_b - x} \rightarrow y = y_b + \text{slope}(x - x_b) \tag{40}$$

The boundary points for the linearly modeled force-deflection response are  $(\delta_{1c}, \mathbf{F}_c)$  at  $\tau = 0$  and  $(\delta_{1s}, \mathbf{0})$  at  $\tau = \tau_s$ . In looking at the two previous equations, we note that  $y$  is analogous to  $\mathbf{F}(\delta(\tau))$ ,  $x$  is analogous to  $\delta(\tau)$ , the values with the subscript of  $a$  are analogous to the values at  $\tau = 0$  and the values with the subscript of  $b$  are analogous to the values at  $\tau = \tau_s$ . As a result:

$$\mathbf{F} = \mathbf{F}_c + \bar{k}(\delta_1 - \delta_{1c}) \tag{41}$$

$$\mathbf{F} = \mathbf{F}_s + \bar{k}(\delta_1 - \delta_{1s}) = \bar{k}(\delta_1 - \delta_{1s}) \tag{42}$$

The modeled IWR can be obtained by multiplying the collision force by the differential of the deflection and integrating over the domain.

$$\begin{aligned}
IWR &= - \int_{\delta_{1c}}^{\delta_{1s}} \mathbf{F} d\delta_1 \\
&= \frac{1}{2} (\delta_{1c} - \delta_{1s}) (2\mathbf{F}_c + \bar{k}(\delta_{1s} - \delta_{1c})) \\
&= \frac{1}{2} (\delta_{1c} - \delta_{1s}) \left( 2\mathbf{F}_c + \frac{\mathbf{0} - \mathbf{F}_c}{\delta_{1s} - \delta_{1c}} (\delta_{1s} - \delta_{1c}) \right) \\
&= \frac{1}{2} \mathbf{F}_c (\delta_{1c} - \delta_{1s})
\end{aligned} \tag{43}$$

The linear separation phase model is defined by a single parameter. Just as with the linear closure phase, the problem is overdetermined. A number of approaches may again be utilized. For all approaches, it is taken as a given that the terminus of closure values are known, irrespective of how they were determined.

1. Determine  $\delta_{1s} = \mathbf{u}_{1s}$  from the data (at  $t_s$ ) and calculate the modeled separation phase stiffness, circular frequency, time of separation and IWR.
2. Use the known IWR to calculate the modeled value of  $\delta_{1s}$  from equation (43) followed by calculation of the modeled separation phase stiffness, circular frequency and time of separation.
3. Use the data to determine  $\tau_s$ , calculate the separation phase modeled circular frequency, stiffness, terminus deflection (residual) and IWR.

With the linear model for the separation phase covered, we proceed with considering the power law model for the separation phase.

#### 2.4 Power separation phase force-deflection model

For the power law model for the separation phase, we first note that the form of the relationship shown by equation (19) is inadequate. As a first option, we consider the form of equation (39) and replace the terms with the corresponding terms from the power law formulation.

$$\ln(\mathbf{F}) = \ln(\mathbf{F}_c) + \bar{a}_1 (\ln(\delta_1) - \ln(\delta_{1c})) \quad (44)$$

Rearranging this equation using equations (21) and (22) leads to the following result.

$$\ln\left(\frac{\mathbf{F}}{\mathbf{F}_c}\right) = \ln\left(\left(\frac{\delta_1}{\delta_{1c}}\right)^{\bar{a}_1}\right) \quad (45)$$

Exponentiating both sides of the equality leads to the following result.

$$\frac{\mathbf{F}}{\mathbf{F}_c} = \left(\frac{\delta_1}{\delta_{1c}}\right)^{\bar{a}_1} \quad (46)$$

The form shown in equation (46), rather than that shown in equation (44), may aid in showing the problem with this formulation when  $\delta_1 = \delta_{1s}$ . The corresponding force value is  $\mathbf{F}_s = \mathbf{0}$ . This value, when used in equation (44), results in the term on the left of the equality becoming negative infinity. When used in equation (46), the term on the left of the equality reduces to zero. However, neither the residual deflection nor the peak deflection are zero valued, thereby making the equation incorrect. Setting this issue aside for the moment, if one were to use equation (46) to determine the IWR:

$$\begin{aligned} \text{IWR} &= - \int_{\delta_{1c}}^{\delta_s} \mathbf{F} \cdot d\delta_1 = - \int_{\delta_{1c}}^{\delta_{1s}} \mathbf{F}_c \left( \frac{\delta_1}{\delta_{1c}} \right)^{\bar{a}_1} \cdot d\delta_1 \\ &= \frac{\mathbf{F}_c}{\delta_{1c}^{\bar{a}_1} (\bar{a}_1 + 1)} \left( \delta_{1c}^{\bar{a}_1 + 1} - \delta_{1s}^{\bar{a}_1 + 1} \right) \end{aligned} \quad (47)$$

For this model, when the IWR,  $\mathbf{F}_c$ ,  $\delta_{1c}$  and  $\delta_{1s}$  are known, the solution for the separation phase power must be determined numerically.

A second option for the form of a power law separation phase model is a horizontally shifted model:

$$\mathbf{F} = \bar{a}_0 (\delta_1 - \delta_{1s})^{\bar{a}_1} \quad (48)$$

This form correctly predicts a value of force of  $\mathbf{F}_s = \mathbf{0}$  when  $\delta_1 = \delta_{1s}$ . When  $\delta_1 = \delta_{1c}$ ,  $\mathbf{F} = \mathbf{F}_c$ , which allows for the following solution:

$$\bar{a}_0 = \frac{\mathbf{F}_c}{(\delta_{1c} - \delta_{1s})^{\bar{a}_1}} \quad (49)$$

Substitution of this result into equation (48) leads to the following result:

$$\mathbf{F} = \frac{\mathbf{F}_c}{(\delta_{1c} - \delta_{1s})^{\bar{a}_1}} (\delta_1 - \delta_{1s})^{\bar{a}_1} \quad (50)$$

The IWR, based upon this formulation, is:

$$\begin{aligned} \text{IWR} &= - \int_{\delta_{1c}}^{\delta_{1s}} \mathbf{F} \cdot d\delta_1 \\ &= - \int_{\delta_{1c}}^{\delta_{1s}} \left( \frac{\mathbf{F}_c}{(\delta_{1c} - \delta_{1s})^{\bar{a}_1}} (\delta_1 - \delta_{1s})^{\bar{a}_1} \right) \cdot d\delta_1 \\ &= \frac{\mathbf{F}_c}{(\delta_{1c} - \delta_{1s})^{\bar{a}_1}} \left( \frac{(\delta_{1c} - \delta_{1s})^{\bar{a}_1 + 1}}{\bar{a}_1 + 1} \right) \\ &= \frac{\mathbf{F}_c}{\bar{a}_1 + 1} (\delta_{1c} - \delta_{1s}) \end{aligned} \quad (51)$$

For this model, when the IWR,  $\mathbf{F}_c$ ,  $\delta_{1c}$  and  $\delta_{1s}$  are known, the solution for the separation phase power can readily be determined in closed form as:

$$\bar{a}_1 = \frac{\mathbf{F}_c}{\text{IWR}} (\delta_{1c} - \delta_{1s}) - 1 \quad (52)$$

A third option for the form of a power law separation phase model is a horizontally and vertically shifted model.

$$\mathbf{F} = \bar{F}_0 + \bar{a}_0 (\delta_1 - \delta_{1c})^{\bar{a}_1} \quad (53)$$

At  $\delta_1 = \delta_{1c}$ :

$$\mathbf{F}_c = \bar{F}_0 + \bar{a}_0 (\delta_{1c} - \delta_{1c})^{\bar{a}_1} \rightarrow \bar{F}_0 = \mathbf{F}_c \quad (54)$$

At  $\delta_1 = \delta_{1s}$ :

$$\mathbf{F} = \mathbf{0} = \bar{F}_0 + \bar{a}_0 (\delta_{1s} - \delta_{1c})^{\bar{a}_1} \rightarrow \bar{a}_0 = -\frac{\bar{F}_0}{(\delta_{1s} - \delta_{1c})^{\bar{a}_1}} \quad (55)$$

Substitution of the results from equations (54) and (55) into equation (53) leads to the following result:

$$\mathbf{F} = \mathbf{F}_c \left( 1 - \frac{(\delta_{1c} - \delta_{1s})^{\bar{a}_1}}{(\delta_{1s} - \delta_{1c})^{\bar{a}_1}} \right) \quad (56)$$

The IWR for this formulation is:

$$\begin{aligned} \text{IWR} &= - \int_{\delta_{1c}}^{\delta_{1s}} \mathbf{F} \cdot d\delta_1 \\ &= - \int_{\delta_{1c}}^{\delta_{1s}} \left( \mathbf{F}_c \left( 1 - \frac{(\delta_{1c} - \delta_{1s})^{\bar{a}_1}}{(\delta_{1s} - \delta_{1c})^{\bar{a}_1}} \right) \right) \cdot d\delta_1 \quad (57) \\ &= \mathbf{F}_c \left( \frac{\bar{a}_1}{\bar{a}_1 + 1} \right) (\delta_{1c} - \delta_{1s}) \end{aligned}$$

For this model, when the IWR,  $\mathbf{F}_c$ ,  $\delta_{1c}$  and  $\delta_{1s}$  are known, the solution for the separation phase power can be determined as:

$$\bar{a}_1 = \left( \frac{\mathbf{F}_c}{\text{IWR}} (\delta_{1c} - \delta_{1s}) - 1 \right)^{-1} \quad (58)$$

For the first formulation, substitution of  $\{\delta_{1c}, \mathbf{F}_c\}$  into equation (46) leads to the result of  $1 = 1$ . For the second formulation, substitution of the same data point into equation (50) leads to the result of  $\mathbf{F}_c = \mathbf{F}_c$ . The same result is obtained by substitution of the same data point into equation (56) in regards to the third formulation. Thusly, if a power law model is used for the closure phase followed by the use of another power law model for the separation phase, one must find a different method of relating the models outside of the force balance that must be present at the contemporaneous terminus of closure and start of separation. The approach taken herein is to use the square of the coefficient of restitution, which, for the subject FRMB impact case, is the ratio of the IWR to the IWA. For the first model, the ratio of equation (47) to equation (29) results in the following relationship between the terminus of closure and terminus of separation deflection values:

$$\delta_{1c} = \delta_{1s} \left( \frac{a_1 + 1}{a_1 - \varepsilon^2 \bar{a}_1 + 1 - \varepsilon^2} \right)^{(\bar{a}_1 + 1)^{-1}} \quad (59)$$

For the second model, the ratio of equation (51) to equation (29) leads to the following:

$$\delta_{1c} = \delta_{1s} \left( 1 - \varepsilon^2 \left( \frac{\bar{a}_1 + 1}{a_1 + 1} \right) \right)^{-1} \quad (60)$$

For the third model, the ratio of equation (57) to equation (29) leads to the following:

$$\delta_{1c} = \delta_{1s} \left( 1 - \varepsilon^2 \left( \frac{\bar{a}_1 + 1}{\bar{a}_1 (a_1 + 1)} \right) \right)^{-1} \quad (61)$$

The results of each of the last three equations can be substituted into equation (19) written at  $\{\delta_{1c}, \mathbf{F}_c\}$ . For the first model:

$$\mathbf{F}_c = a_0 \left( \frac{a_1 + 1}{a_1 - \varepsilon^2 \bar{a}_1 + 1 - \varepsilon^2} \right)^{a_1 (\bar{a}_1 + 1)^{-1}} \delta_{1s}^{a_1} \quad (62)$$

For the second model:

$$\mathbf{F}_c = a_0 \left( 1 - \varepsilon^2 \left( \frac{\bar{a}_1 + 1}{a_1 + 1} \right) \right)^{-a_1} \delta_{1s}^{a_1} \quad (63)$$

For the third model:

$$\mathbf{F}_c = a_0 \left( 1 - \varepsilon^2 \left( \frac{\bar{a}_1 + 1}{\bar{a}_1 (a_1 + 1)} \right) \right)^{-a_1} \delta_{1s}^{a_1} \quad (64)$$

For each of these three relationships, it can readily be seen that the form is of a constant multiplied by the terminus of separation deflection raised to the  $a_1$  power. Thusly, these relationships are log-linear as was the relationship given by equation (19).

## 2.5 Power law kinematic response

It was previously noted that the differential equation of motion for this model, given by equation (27), is nonlinear and not amenable to being solved for in closed form. We may, however, determine an approximate solution using a numerical method. Direct time integration, using the explicit central difference method, is used herein. We start with the Taylor series expansion of a function  $f(x)$  at  $x = a$ , which can be written as:

$$f(x) = \sum_{n=0}^{\infty} \frac{f^{(n)}(a)}{n!} (x-a)^n \quad (65)$$

Where  $f^{(n)}(a)$  is the  $n^{\text{th}}$  derivative of  $f(x)$  evaluated at  $x = a$ . Expanding the summation leads to the following:

$$f(x) = f(a) + \left. \frac{df}{dx} \right|_{x=a} (x-a) + \left. \frac{1}{2} \frac{d^2 f}{dx^2} \right|_{x=a} (x-a)^2 + \dots \quad (66)$$

Replacing  $x$  with the displacement  $\mathbf{u}$ , replacing  $a$  with  $t_i$ , which denotes the time at the  $i^{\text{th}}$  time step and replacing  $x$  with  $t$  leads to the following form:

$$\mathbf{u}(t) = \mathbf{u}(t_i) + \left. \frac{d\mathbf{u}}{dt} \right|_{t=t_i} (t-t_i) + \left. \frac{1}{2} \frac{d^2 \mathbf{u}}{dt^2} \right|_{t=t_i} (t-t_i)^2 + \dots \quad (67)$$

When  $t = t_i + \Delta t$ , equation (67) becomes:

$$\mathbf{u}(t_i + \Delta t) = \mathbf{u}(t_i) + \left. \frac{d\mathbf{u}}{dt} \right|_{t=t_i} \Delta t + \left. \frac{1}{2} \frac{d^2 \mathbf{u}}{dt^2} \right|_{t=t_i} \Delta t^2 + \dots \quad (68)$$

When  $t = t_i - \Delta t$ , equation (67) becomes:

$$\mathbf{u}(t_i - \Delta t) = \mathbf{u}(t_i) - \frac{d\mathbf{u}}{dt} \Big|_{t=t_i} \Delta t + \frac{1}{2} \frac{d^2\mathbf{u}}{dt^2} \Big|_{t=t_i} \Delta t^2 + \dots \quad (69)$$

Switching to the overdot notation, truncating equations (68) and (69) to the first two terms followed by the subtraction of the former from the latter leads to the following:

$$\dot{\mathbf{u}}(t_i) = \frac{\mathbf{u}(t_i + \Delta t) - \mathbf{u}(t_i - \Delta t)}{2\Delta t} \quad (70)$$

Truncating the same two equations to their first three terms followed by addition leads to the following:

$$\ddot{\mathbf{u}}(t_i) = \frac{\mathbf{u}(t_i + \Delta t) - 2\mathbf{u}(t_i) + \mathbf{u}(t_i - \Delta t)}{\Delta t^2} \quad (71)$$

Substitution of equation (71) into equation (27) followed by rearrangement leads to the following solution:

$$\mathbf{u}(t_i + \Delta t) = 2\mathbf{u}(t_i) + \frac{a_0}{m} \Delta t^2 (\mathbf{u}_1(t_i))^{\bar{a}_1} - \mathbf{u}(t_i - \Delta t) \quad (72)$$

For the first timestep, the solution for the displacement at the second timestep, requires the solution for the previous timestep. This can be determined by solving equation (70) for the displacement  $\mathbf{u}(t_i + \Delta t)$ , substituting the result into equation (71) and rearranging (for this,  $i = 1, t = t_o = 0$ ).

$$\mathbf{u}(-\Delta t) = \mathbf{u}(t_o) - \Delta t \dot{\mathbf{u}}(t_o) + \frac{\Delta t^2}{2} \ddot{\mathbf{u}}(t_o) \quad (73)$$

For each time step, we first solve for the displacement at the next time step using equation (72) and then solve for the velocity and acceleration at the current time step using equations (70) and (71), respectively. Equation (72) is the correct equation for the closure phase. Once the velocity of the vehicle becomes negative, the form of this equation changes based upon the separation phase model of choice. For the first separation phase model, the displacement solution becomes:

$$\mathbf{u}(t_i + \Delta t) = 2\mathbf{u}(t_i) + \frac{\mathbf{F}_c \Delta t^2}{m \delta_{1c}^{\bar{a}_1}} (\mathbf{u}_1(t_i))^{\bar{a}_1} - \mathbf{u}(t_i - \Delta t) \quad (74)$$

For the second separation phase model, the displacement solution becomes:

$$\begin{aligned} \mathbf{u}(t_i + \Delta t) &= 2\mathbf{u}(t_i) + \frac{\mathbf{F}_c \Delta t^2}{m (\delta_{1c} - \delta_{1s})^{\bar{a}_1}} (\mathbf{u}_1(t_i) - \delta_{1s})^{\bar{a}_1} \\ &\quad - \mathbf{u}(t_i - \Delta t) \end{aligned} \quad (75)$$

For the third separation phase model, the displacement solution becomes:

$$\begin{aligned} \mathbf{u}(t_i + \Delta t) &= 2\mathbf{u}(t_i) + \frac{\mathbf{F}_c \Delta t^2}{m} \left( 1 - \frac{(\mathbf{u}(t_i) - \delta_{1c})^{\bar{a}_1}}{(\delta_{1s} - \delta_{1c})^{\bar{a}_1}} \right) \\ &\quad - \mathbf{u}(t_i - \Delta t) \end{aligned} \quad (76)$$

It should be readily apparent that only the first model does not require *a priori* knowledge of the terminus of separation deflection.

### 3. METHODS AND MATERIALS

The models developed above were evaluated, on a preliminary basis, using data generated from a pair of controlled collision tests. The first test was NHTSA test number v03196, conducted as a baseline test, involving a frontal impact between a 1995 Chevrolet Lumina LS APV minivan (VIN: 2G1WN52XS9243954, transverse 3.4 liter six cylinder engine, four speed automatic front wheel drive, mass = 1781 kg) and an instrumented FRMB (36 load cells arranged in four rows and nine columns). The second test was NHTSA test number v01990, conducted as a NCAP test, involving a frontal impact between a 1994 Pontiac Trans Sport minivan (VIN: 1GMDU06D5RT202095, transverse 3.1 liter six cylinder engine, three speed automatic front wheel drive, mass = 1962 kg) and an instrumented FRMB (configuration as per the previous). This pair of tests was chosen secondary to the former being a lower speed impact test (impact speed of 24.0 KPH) and the latter being a higher speed impact test (impact speed of 56.5 KPH) for the same vehicle platform.

The platform determination was based upon an examination of the components of the salient subsystems as documented by the parts catalog information produced by Mitchell International, Inc. (San Diego, California, USA). The structural components, for the platform year range of 1994-1996, were the same for the front inner structure, side structure (including the rails) and subframe. The components comprising the front suspension were substantially similar. Differences were noted with respect to the front bumper system. The part numbers differed for the impact absorber (referenced as such for the Chevrolet and referenced as a reinforcement for the Pontiac) and the impact bar. The part numbers for the front bumper mounting brackets were the same (referenced as impact bar reinforcements for the Chevrolet and as impact bar plates for the Pontiac).

For each test, the instrumentation data in NHTSA EV5 ASCII X-Y format, was imported directly from the NHTSA website. For each test, the EV5 file was imported into a symbolic mathematics software package (Mathematica v. 12.0; Wolfram Research, Inc.; Champaign, Illinois, USA). The same software package was used for all data reductions. The EV5 file was parsed using a custom written program that utilized the standardized EV5 data element designations. The load

cell barrier instrumentation file names were extracted using string pattern matching. Each file was individually imported and filtered using a custom written Society of Automotive Engineers (SAE) channel frequency class (CFC) 60 filter. The data prior to time  $t = t_0 = 0$  was discarded followed by transposing 100 milliseconds of data, at the start and end of the signal, about  $(0, 0)$ , for signal padding. This padded signal was passed through the digital filter forward and then in reverse followed by discarding of the padding.

The filtered load cell data was summed, at each time point, to generate the total barrier force time history. The discrete time-deceleration history for the test vehicle was determined by dividing the total barrier force, at each time point, by the mass of the test vehicle. The discrete time-velocity and displacement of the test vehicle, with the displacement equating to the deflection for the FRMB impact case, was determined by numerically integrating the time-deceleration history. As expected, the velocity did not reach a zero value at a sampled data point but instead reached that value between a pair of immediately adjacent data points. This was also case for the acceleration in regards to the separation phase analysis. For both the velocity and the acceleration, the data points that bounded the zero value were used to generate a linear interpolation function and determine the time at which the abscissa was crossed. The same indices for the other kinematic responses were then linearly interpolated and solved at the time values at which the abscissa was crossed from the previous step.

The linear model for the closure phase was evaluated in accordance with the four methods described in Section 2.1. The linear model for the separation phase was evaluated in accordance with the three methods described in Section 2.3. The power law model for the closure phase consisted of using equation (30) to determine the power value and using equation (28) to determine the coefficient value. The power law model for the separation phase was implemented for each of the three methods detailed in Section 2.4. Finally, the numerically integrated kinematic response, for the power law model, was determined using equation (72) for the closure phase displacement and equation (74) for the separation phase displacement.

#### 4.RESULTS

The data reduction for both collision tests, as expected, produced total barrier force time histories that were indicative, even under the modeling constraints of uniaxiality, of a multiple degree of freedom (MDOF) system response. This is clearly evidenced by multiple, interval, substantive, extrema rather than a singular extremum. The total barrier force time history for both tests is shown in Figure 2. For the lower speed test (i.e. v03196), the closure phase parameters were determined to be the following:  $t_c = 85.83$  msec,  $\mathbf{u}_{1c} = \boldsymbol{\delta}_{1c} = 0.3732$  m,  $\mathbf{a}_{1c} = -122.1$  m/sec<sup>2</sup>,  $\mathbf{F}_c = 2.174 \cdot 10^5$  N and IWA =  $3.958 \cdot 10^4$  J. The closure phase

parameters for the higher speed test (i.e. v01990) were determined to be the following:  $t_c = 99.90$  msec,  $\mathbf{u}_{1c} = \boldsymbol{\delta}_{1c} = 0.8244$  m,  $\mathbf{a}_{1c} = -96.40$  m/sec<sup>2</sup>,  $\mathbf{F}_c = 1.891 \cdot 10^5$  N and IWA =  $2.416 \cdot 10^5$  J.

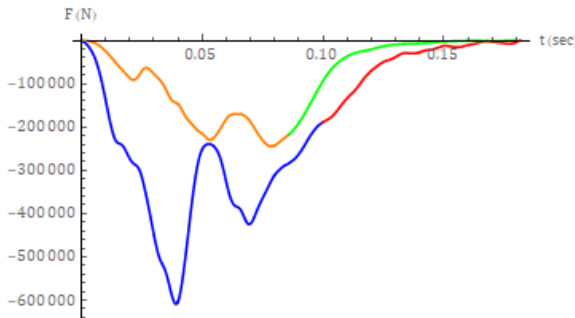


**Fig -2:** Total barrier force time histories for test v01990 (blue for closure, red for separation) and test v03196 (orange for closure, green for separation)

The separation phase parameters for the lower severity collision test were determined to be the following:  $t_s = 179.2$  msec ( $\tau_s = 93.34$  msec),  $\mathbf{u}_{1s} = \boldsymbol{\delta}_{1s} = 0.2186$  m,  $\mathbf{v}_{1s} = -1.943$  m/sec and IWR =  $3.361 \cdot 10^3$  J. The separation phase parameters for the higher severity collision test were determined to be the following:  $t_s = 181.6$  msec ( $\tau_s = 81.71$  msec),  $\mathbf{u}_{1s} = \boldsymbol{\delta}_{1s} = 0.6952$  m,  $\mathbf{v}_{1s} = -2.024$  m/sec and IWR =  $4.018 \cdot 10^3$  J. The coefficient of restitution for the lower severity test was -0.2914 and for the higher severity test was -0.1290. The acceleration, velocity and displacement (deflection) time histories, for both tests, are shown in Figures 3-5, respectively.

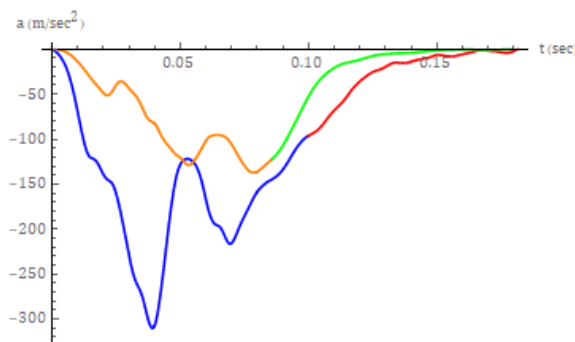


**Fig -3:** Acceleration time histories for test v01990 (blue for closure, red for separation) and test v03196 (orange for closure, green for separation)

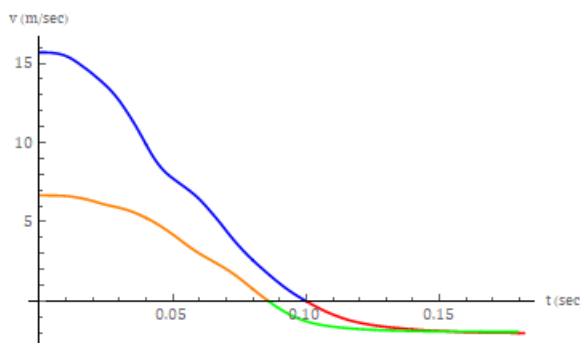


**Fig -4:** Velocity time histories for test v01990 (blue for closure, red for separation) and test v03196 (orange for closure, green for separation)

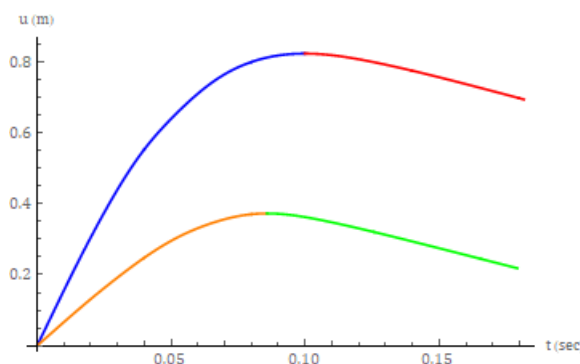


**Fig -5:** Displacement (deflection) time histories for test v01990 (blue for closure, red for separation) and test v03196 (orange for closure, green for separation)

The acceleration time histories mirror the total barrier force time histories, as expected, given that the former are merely the latter scaled, along the ordinate, by the inverse of the mass of the corresponding test vehicle. The responses for both collision severities were similar. The initial increase in the response magnitude was followed by a slight drop in the lower severity test and a region of reduced slope in the higher severity test. This was then followed by a double peak response, with an interposed local minimum, followed by a relatively lengthy tail response. The peak force magnitude, for both cases, occurred during closure rather than at the terminus of closure. The smoothing effect of integration can readily be seen in the velocity time histories shown in Figure 4 and the displacement (deflection) responses shown in Figure 5. For both tests, the peak deflection occurred at the terminus of closure. The force-deflection response for the two tests is shown in Figure 6.

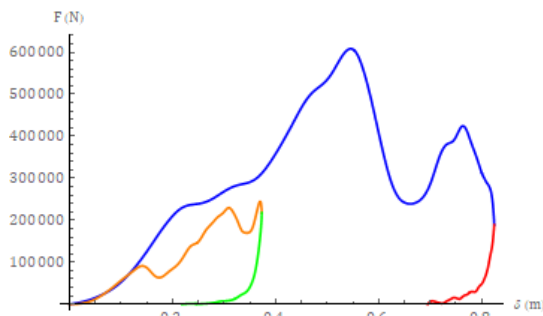


**Fig -6:** Force-deflection responses for test v01990 (blue for closure, red for separation) and test v03196 (orange for closure, green for separation)

The force-deflection response for both tests is quite similar, but not an exact overlay, over approximately the first 0.130 meters of deflection. The local minimum seen in the acceleration response for the lower severity test and the region of reduced slope seen in the higher severity test are both manifested in the force-deflection response. For the lower severity test, the peak force magnitude occurs with the second peak of the double peak response. For the higher severity test, the peak force magnitude occurs with the first peak of the double peak response. The peak deflection, for the lower severity case, occurs much closer to the peak collision force, when compared to the higher severity test.

The linear model fits for the closure phase force-deflection response for the higher severity collision test are shown in Figure 7. The first model, based upon the known values for  $\delta_{1c}$  and  $F_c$ , resulted in values for  $k$ ,  $\omega$ ,  $t_c$  and the IWA of  $2.294 \cdot 10^5$  N/m,  $10.81 \text{ sec}^{-1}$ ,  $145.3$  msec and  $7.796 \cdot 10^4$  J, respectively. The second model, based upon the known values for  $\delta_{1c}$  and the IWA resulted in values for  $k$ ,  $\omega$ ,  $t_c$  and  $F_c$  of  $7.110 \cdot 10^5$  N/m,  $19.04 \text{ sec}^{-1}$ ,  $82.52$  msec and  $5.862 \cdot 10^5$  J. The third model, based upon the known time at which the closure phase terminates, resulted in values for  $k$ ,  $\omega$ ,  $\delta_{1c}$ ,  $F_c$  and IWA of  $4.851 \cdot 10^5$  N/m,  $15.72 \text{ sec}^{-1}$ ,  $9.981 \cdot 10^{-1}$  m,  $4.842 \cdot 10^5$  N and  $2.416 \cdot 10^5$  J, respectively.

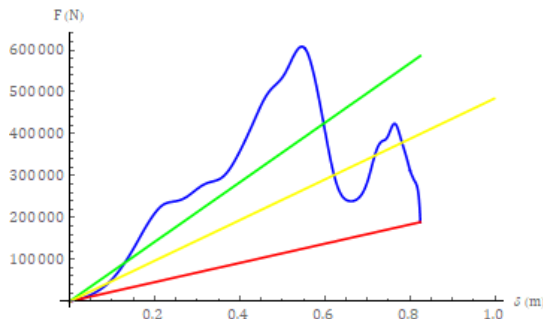


**Fig -7:** Closure phase force-deflection response for test v01990 (blue) with the first, second and third models, as per the text, shown by the red, green and yellow curves, respectively.

The linear model fits for the closure phase force-deflection response for the lower severity collision test are shown in Figure 8. The first model, based upon the known values for  $\delta_{1c}$  and  $F_c$ , resulted in values for  $k$ ,  $\omega$ ,  $t_c$  and the IWA of  $5.827 \cdot 10^5$  N/m,  $18.09 \text{ sec}^{-1}$ ,  $86.84$  msec and  $4.0571 \cdot 10^4$  J, respectively. The second model, based upon the known values for  $\delta_{1c}$  and the IWA resulted in values for  $k$ ,  $\omega$ ,  $t_c$  and  $F_c$  of  $5.684 \cdot 10^5$  N/m,  $17.87 \text{ sec}^{-1}$ ,  $87.92$  msec and  $2.121 \cdot 10^5$  J. The third model, based upon the known time at which the closure phase terminates, resulted in values for  $k$ ,  $\omega$ ,  $\delta_{1c}$ ,  $F_c$  and IWA of  $5.965 \cdot 10^5$  N/m,  $18.30 \text{ sec}^{-1}$ ,  $3.643 \cdot 10^{-1}$  m,  $2.173 \cdot 10^5$  N and  $3.958 \cdot 10^4$  J, respectively.

For the separation phase of the lower severity test, the three linear models consisted of (1) using  $\delta_{1s}$  from  $t_s$ , (2) using the IWR and (3) using  $\tau_s$ . For the first case, the modeled values for the stiffness, circular frequency,  $\tau_s$  and IWR are  $1.407 \cdot 10^6$  N/m,  $28.10 \text{ sec}^{-1}$ ,  $55.90$  msec and  $3.360 \cdot 10^4$  J, respectively. For the second case, the modeled values for the stiffness, circular frequency,  $\delta_{1s}$  and  $\tau_s$  are  $7.033 \cdot 10^6$  N/m,  $62.84 \text{ sec}^{-1}$ ,  $3.422 \cdot 10^{-1}$  m and  $25.00$  msec, respectively. For the third case, the modeled values for the stiffness, circular frequency,  $\delta_{1s}$  and IWR are  $5.043 \cdot 10^5$  N/m,  $16.83 \text{ sec}^{-1}$ ,  $-5.796 \cdot 10^{-2}$  m and  $4.687 \cdot 10^4$  J, respectively. These results are shown in Figure 9.

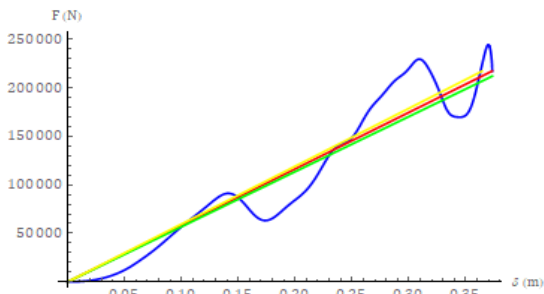


**Fig -8:** Closure phase force-deflection response for test v03196 (blue) with the first, second and third models, as per the text, shown by the red, green and yellow curves, respectively.

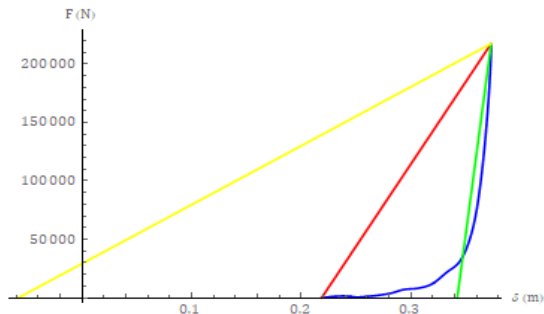


**Fig -9:** Separation phase force-deflection response for test v03196 (blue) with the first, second and third models, as per the text, shown by the red, green and yellow curves, respectively.

For the higher severity test, the modeled values generated by the first case, for the stiffness, circular frequency,  $\tau_s$  and IWR are  $1.463 \cdot 10^6$  N/m,  $27.31 \text{ sec}^{-1}$ ,  $57.52$  msec and  $3.536 \cdot 10^5$  J, respectively. For the second case, the modeled values for the stiffness, circular frequency,  $\delta_{1s}$  and  $\tau_s$  are  $4.451 \cdot 10^6$  N/m,  $47.63 \text{ sec}^{-1}$ ,  $7.820 \cdot 10^{-1}$  m and  $32.98$  msec, respectively. For the third case, the modeled values for the stiffness, circular frequency,  $\delta_{1s}$  and IWR are  $7.251 \cdot 10^5$  N/m,  $19.22 \text{ sec}^{-1}$ ,  $5.636 \cdot 10^{-1}$  m and  $2.467 \cdot 10^4$  J, respectively. These results are shown in Figure 10.

The power law model, as a singular model for the closure phase of the higher severity collision test, based upon the data, failed to meet the required criterion of  $(F_c \delta_{1c}) / \text{IWA} > 1$ . The value of the evaluated term on the left of the inequality was determined to be 0.6453. For the lower severity collision test, the value of this term was determined to be 2.050, which resulted in a value of  $a_0 = 6.123 \cdot 10^5$  (units of N per meter raised to the  $a_1$  power) and an  $a_1$  value of 1.050. The overlay of this model, upon the closure phase data, is shown graphically in Figure 11.

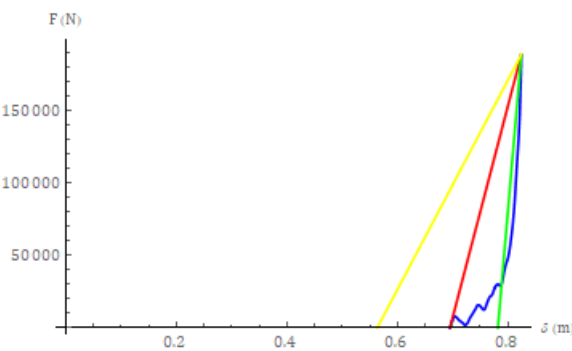


**Fig -10:** Separation phase force-deflection response for test v01990 (blue) with the first, second and third models, as per the text, shown by the red, green and yellow curves, respectively.

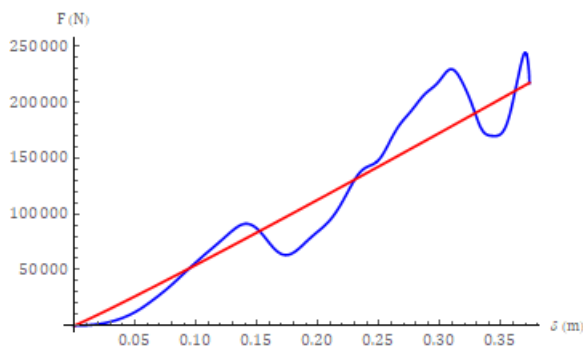


**Fig -11:** Closure phase force-deflection response for test v03196 (blue) with the power law model fit overlaid (red).

For the higher severity collision test, the separation phase power law model exemplified by equation (46) resulted in a power term of 37.75 and with a residual force magnitude, at the terminus of separation, of 302.5 N. The second model, for this test, exemplified by equation (50) resulted in a power term of 5.084. The third model, for this test, exemplified by equation (56) resulted in a power term of  $1.967 \cdot 10^{-1}$ . The three model fits to the separation phase force-deflection response are shown in Figure 12.

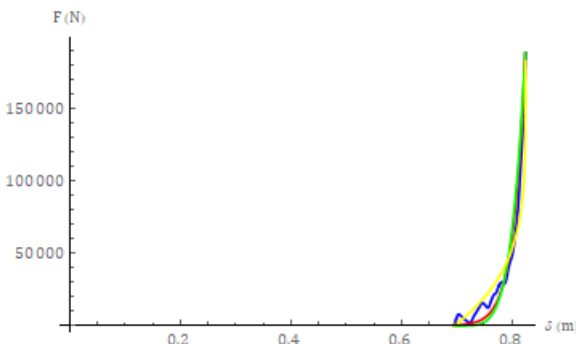


**Fig -12:** Separation phase force-deflection response for test v01990 (blue) with the first, second and third models, as per the text, shown by the red, green and yellow curves, respectively.

For the lower severity test, the first model produced a power term of 23.14 and with a residual force magnitude of  $9.147 \cdot 10^{-1}$  N. The second model produced a power term of 9.001. The third model produced a power term of  $1.111 \cdot 10^{-1}$ . The three model fits to the separation phase force-deflection response are shown in Figure 13.

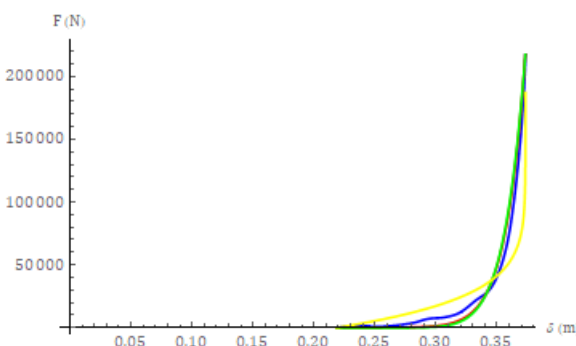


**Fig -13:** Separation phase force-deflection response for test v03196 (blue) with the first, second and third models, as per the text, shown by the red, green and yellow curves, respectively.

For the lower severity collision test, the modeled kinematic response, based upon the power law model for the closure phase followed by a power law model for the separation phase, was evaluated by means of numerical integration. Because there was only one model for the closure phase, the differences in the modeled kinematics were due to the three different power law models for the separation phase. The

models are referenced as before. For the first model, the values of  $t_s$ ,  $\delta_{1s}$ , velocity at separation and acceleration at separation are 177.8 msec,  $2.182 \cdot 10^{-1}$  m, -1.943 m/sec and - $4.935 \cdot 10^{-4}$  m/sec $^2$ , respectively. The values for the second model are 182.9 msec,  $2.078 \cdot 10^{-1}$  m, -1.943 m/sec and 0 m/sec $^2$ , respectively. Finally, for the third model, the values are 194.6 msec,  $2.186 \cdot 10^{-1}$  m, -1.943 m/sec and 0 m/sec $^2$ . The results are shown, graphically, for the acceleration, velocity and displacement, in Figures 14-16, respectively.

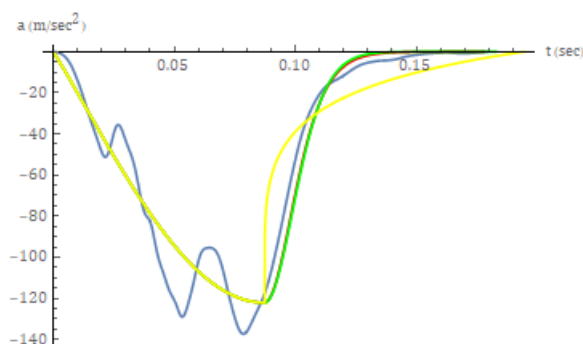


**Fig -14:** Acceleration-time history for test v03196 (blue) with the first, second and third models, as per the text, shown by the red, green and yellow curves, respectively.

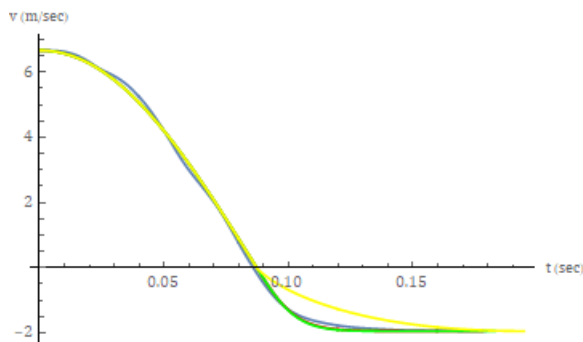


**Fig -15:** Velocity-time history for test v03196 (blue) with the first, second and third models, as per the text, shown by the red, green and yellow curves, respectively.

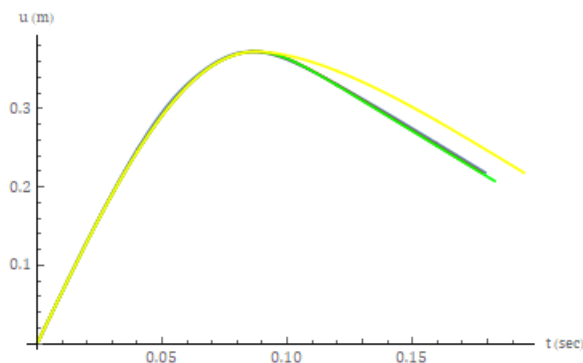


**Fig -16:** Displacement-time history for test v03196 (blue) with the first, second and third models, as per the text, shown by the red, green and yellow curves, respectively.

## 5.DISCUSSION

Residual damage based methods can readily be viewed as one of the simplest approaches for determining quantitative estimates for motor vehicle collision severity. For model parameter quantification from controlled collision test data, the data reduction process does not require the evaluation of any of the dynamic instrumentation data that is generated during the collision test. In contrast, even the simplest dynamic modeling approaches require significant, albeit readily implementable, data reduction. The SDOF models presented in this work fall within this classification. This statement is made because of the use of ubiquitous uniaxiality coupled with a single lumped mass for the test vehicle. The first condition, as noted previously, greatly simplifies the analysis by removing the necessity for determining the time-varying DCM for each local frame of reference that is salient to the analysis. The second condition reduces the number of second order differential equations of motion to unity.

The MDOF nature of the system response during closure, even for the uniaxial approximation, can readily be seen by simple examination of Figure 6. This is exemplified by the local extrema and lack of a ubiquitous monotonic response. These local responses are due to frontal subsystems such as the front bumper system, front frame, engine and the front wheels and suspension. The impact of these subsystems, within the context of a SDOF modeling approach, is variable. For the lower severity collision test, as shown in Figure 8, the deviation of the response from the case of a purely monotonically increasing function is limited and the force at the terminus of the closure phase is close in magnitude to the peak force. Thusly, the three linear fits are closely approximated to each other as well to the actual response (when compared with the higher collision severity test). This was clearly not the case for the closure phase of the higher severity collision test. Visual inspection of Figures 2 and 3 shows that the peak force and acceleration occur relatively early during the closure phase. This is then manifested with a peak force that occurs prior to the peak deflection as seen in Figures 6 and 7. From the latter, it can readily be seen that the three linear closure phase models diverge. Furthermore, none of the models provides a good fit for the data.

One of the findings of the subject work, which is a novel finding with respect to the application context, is that the power law model, as a single model for the entirety of the closure phase, has a limitation based upon the inequality  $F_c \delta_c / IWA > 1$ . This inequality did not hold for the higher severity collision test considered in the subject work. One may readily make the statement that collision tests with closure phase force-deflection responses that are similar to the response of the subject higher severity collision test, in regards to an early peak force magnitude and relatively low force magnitude at the terminus of closure, would also result

in the inequality not holding. This statement is based upon deterministic considerations. One may further state that the set of characteristics found in the closure phase response of the higher severity collision test represent one class, but not necessarily the only class, of response for which the inequality would not hold. The lower severity collision test, on the other hand, provided data for which the inequality held. The closure phase power law fit, however, was very close to being linear. It is unclear if this approximate linear fit represents a limitation on the use of a single power law function for modeling the closure phase.

Two additional points regarding the closure phase response are worthy of discussion. The first point is that the force-deflection response for the approximate first 0.130 meters of deflection is quite similar between the higher and lower severity collision tests. That such similitude exists over a non-trivial deflection magnitude is more germane than the magnitude itself. The finding shows that the initial portion of the response follows a very similar path for the two collision severities in question. The slight differences can be attributed to differences between the test vehicles, variations associated with the implementation of the testing protocols and response contributions, albeit minor, from other load paths or a combination. The contributions of these other load paths become more substantial in the higher severity collision test, following the initial portion of similitude. The second point is that it is highly unlikely that there would be a substantially different response for a lower severity collision, for the deflection regime starting at zero and terminating at the appropriate value before 0.130 meters of deflection. This statement holds due to the fact the subject lower severity collision test has to 'pass through' the same response regime, engaging the same vehicle frontal systems, in the same manner, for impacts with a lower severity.

For both tests, the linear modeling approach faired quite poorly, as expected, for the separation phase. This was most apparent for the third model, for the higher severity collision test, as shown in Figure 9. Qualitatively, the separation phase response for both tests can be characterized as being biphasic. The first phase of the response consists of a steep drop in the force magnitude with a minimum but finite decrement in the deflection. The second phase of the response consists of a steep decrease in the deflection with a minimum but finite decrement in the collision force. The transition between the two phases is relatively smooth (rather than abrupt). For both tests, the power law modeling approach provided a substantially better fit to the separation response when compared with the linear model fits. For the higher severity collision test, as evidenced by Figure 12, the first and second separation phase power law models were essentially overlayed and provided a better fit to the actual data than the third model. Again, it should be noted that the first model, by its design, does not predict a zero valuation for the force at the terminus of the separation phase. These

findings are also apt for the lower severity collision test, as per Figure 13.

For the lower severity collision test, the first two models for the separation phase, again, were virtually overlayed in regards to kinematic responses shown in Figure 14-16. Both of these models provide a better fit to the actual data when compared to the fit provided by the third model. With respect to the terminus of the closure phase for the collision test, the modeled responses lag the actual response secondary to the former falling between the time steps of the latter. The impact of this is most apparent on the acceleration response as shown in Figure 14. The differences between the actual data and the first two models, in regards to the acceleration response, as expected, are minimized for both the velocity and displacement responses (as per Figures 15 and 16 respectively).

While only two tests were considered in the subject work, there are a number of findings that are of utility when one considers future development. The first, which retains both the SDOF approach and ubiquitous uniaxiality, is the consideration of a multistep power law formulation for the separation phase. This consideration derives from the fact that the model coefficients, for each power law formulation, for the two tests, differed. Ideally, for a given platform and a given model, the model parameters should be the same across all salient collisions that traverse the same severity domain. The second consideration for future development is the development of a MDOF model while retaining ubiquitous uniaxiality. Such an approach would be most useful for collision tests with a closure phase similar to the higher severity test considered in the subject work. This consideration requires evaluation of test vehicle fixed accelerometer data. The third consideration for future development is the relaxation of ubiquitous uniaxiality. This consideration requires one or both of the following two approaches. The first is the use of vehicle fixed accelerometer data. For a typical test, the configuration of the vehicle fixed accelerometer array allows for the determination of biaxial motion, in the x-z plane, for the body of the test vehicle. The second approach for determining the kinematic response of the test vehicle is by means of videogrammetry. In theory, the process can be undertaken using video from a single fixed position camera. However, it is likely that the analysis of video data from multiple camera locations would be the most appropriate for accurately quantifying the response in three dimensions.

## REFERENCES

- [1] D Sharma, S Stern, J Brophy, E-H Choi (2007) An overview of NHTSA's crash reconstruction software WinSMASH. Proceedings: 20<sup>th</sup> International Technical Conference on the Enhanced Safety of Vehicles, Lyon, France (June 18-21, 2007). Paper number 07-0211.
- [2] KL Campbell (1972) Energy as a basis for accident severity – A preliminary study. Doctoral dissertation: Automotive Engineering, University of Wisconsin.
- [3] KL Campbell (1974) Energy basis for collision severity. Society of Automotive Engineers technical paper number 740565.
- [4] RR McHenry (1975) A comparison of results obtained with different analytical techniques for reconstruction of highway accidents. Society of Automotive Engineers technical paper number 750893.
- [5] RI Emori (1968) Analytical approach to automobile collisions. Society of Automotive Engineers technical paper number 680016.
- [6] J Singh (2013) A fundamental reconsideration of the CRASH3 damage analysis algorithm: the case against uniform ubiquitous linearity between BEV, peak collision force magnitude and residual damage depth. Traffic Injury Prevention 14(7): 18-24.
- [7] CE Strother, RL Woolley, MB James and CY Warner (1986) Crush energy in accident reconstruction. Society of Automotive Engineers technical paper number 860371.
- [8] RR McHenry and BG McHenry (1986) A revised damage analysis procedure for the CRASH computer program. Society of Automotive Engineers technical paper number 861894.
- [9] RR McHenry and BG McHenry (1997) Effects of restitution in the application of crush coefficients. Society of Automotive Engineers technical paper number 970960.
- [10] JA Neptune (1998) Crush stiffness coefficients, restitution constants and a revision of CRASH3 and SMAC. Society of Automotive Engineers technical paper number 980029.
- [11] JF Kerkhoff, SE Husher, MS Varat, AM Busenga and K Hamilton (1993) An investigation into vehicle frontal impact stiffness, BEV and repeated testing for reconstruction. Society of Automotive Engineers technical paper number 930899.
- [12] RL Woolley (2001) Non-linear damage analysis in accident reconstruction. Society of Automotive Engineers technical paper number 2001-01-0504.
- [13] J Singh and J Perry (2008) Multilinear and nonlinear power law modeling of motor vehicle force-deflection response for uniaxial front impacts. Accident Reconstruction Journal 18(6): 30-38, 62.

- [14] J Singh (2013) Further developments regarding the dynamic modeling of motor vehicle collision response using the SDOF approach. Collision 8(1): 10-31.
- [15] NJ Carpenter and JB Welcher (2001) Stiffness and crush energy analysis for vehicle collision and its relationship to barrier equivalent velocity (BEV). Society of Automotive Engineers technical paper number 2001-01-0500.

## BIOGRAPHY



Mr. Singh is a private practice engineer with specialties in the fields of motor vehicle accident reconstruction and biomechanical engineering. He holds a BS in mechanical engineering from the University of Illinois at Urbana-Champaign and a MS in biomedical engineering from the University of Southern California. He has authored numerous peer reviewed conference proceeding papers, technical papers and scientific papers